Volume 1 | Number 1 | Jan 2013 | Pages 1–100

Dalton Transactions

An international journal of inorganic chemistry
www.rsc.org/dalton

ROYAL SOCIETY OF CHEMISTRY

ROYAL SOCIETY OF CHEMISTRY

www.rsc.org/dalton

Journal Name

ARTICLE

Hypercoordinate β-Carbon in Grubbs and Schrock Olefin Metathesis Metallacycles

Premaja R. Remya [†,‡] and Cherumuttathu H. Suresh*,[†,‡]

Metallacyclobutane (MCB) intermediates of Grubbs and Schrock olefin metathesis catalysts are well-known for their unusually short single bond-like metal to C_β distance and unusually long $C_\alpha C_\beta$ distances. From the analysis of structural, bond order, electron density and ^{13}C NMR data of a large variety of MCB systems, we show that the C_β of the metallacycle possesses pentacoordinate geometry due to agostic type interaction of the metal with the $C_\alpha C_\beta$ bonds. The pentacoordination of C_β to the metal center is characterized by a catastrophe ring critical point (RCP) in the quantum theory of atoms-in-molecule (QTAIM) analysis. Fine tuning of the ligand environment changes the catastrophe point to a fifth bond critical point (BCP) which is clearly brought out in the case of two ruthenium olefin metathesis systems. Several Ru and W agostic MCB complexes exhibiting pentacoordinate C_β as well as their non-agostic isomers have been reported at the BP86/def2-TZVPP level of DFT. The agostic systems showed significant bond order between metal and C_β (0.17 – 0.36), single bond-like electron density values at the catastrophe RCP/BCP and significantly large difference in ^{13}C NMR chemical shift values between C_α and C_β atoms.

Introduction

The Chauvin mechanism[1] of olefin metathesis, applicable to Grubbs-, Schrock- and other related complexes is one of the most elegant mechanistic pathways known in synthetic organic chemistry for the last five decades.[2-3] This general mechanism suggests the formation of a metallacyclobutane (MCB) as a key intermediate in the reaction (Scheme 1) through a formal [2+2] cyclo-addition between the incoming olefin and the metal-carbon double bond. The olefin coordination to the metal is facilitated by the dissociation of a phosphine or a labile ligand from the catalyst. Though the catalyst and the olefin-coordinated metal complex possess 16-electron configuration, the MCB, due to its +4 oxidation state is formally a 14-electron system. Therefore, in the early development of metathesis mechanism, MCB has been speculated as a transition state whereas later experimental and theoretical studies have confirmed it as an intermediate.[4-33] In 2005, Romero and Piers[14] gave convincing evidence based on ^1H and ^{13}C NMR measurements that 14-electron ruthenacyclobutane intermediate of olefin metathesis is an observable intermediate in N-heterocyclic carbene (NHC)-stabilized Grubbs catalysts. Adlhart et al.[7] and Cavallo[8] provided theoretical explanation for the formation of ruthenacyclobutane in Grubbs olefin metathesis. Formation of

MCB suggests the conversion of MC and CC double bonds to the corresponding single bonds along with the formation of a new CC single bond. In other words, a CC double bond is activated to a single bond during the metallacycle formation. In the subsequent step of cyclo-reversion, one MC and one CC single bonds of the metallacycle are cleaved. Literature shows that the activation barrier for cyclo-reversion is 5 - 10 kcal/mol for Grubbs and Schrock olefin metathesis which is the most noteworthy feature of the mechanism as this value is astonishingly low for the cleavage of a CC single bond.[8, 13, 15, 22, 27, 34-36] Such a low barrier for CC bond cleavage can be justified only if the strength of the CC bonds in MCB is largely deteriorated from a typical CC single bond. On examination of the reported MCB structures of olefin metathesis in the literature for Ru, Ti, Nb, W, Mo and Ta, one could easily identify that the CC bonds of the metallacycles are weak as they show significant elongation ~1.60 Å compared to a normal CC single bond, ~1.52 Å.[15, 37] The substantial activation of CC bonds in the metallacycles explains the low activation barrier for the metathesis reaction.
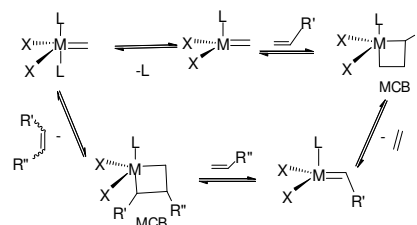
Scheme 1. The general scheme for alkene metathesis reaction.

† Chemical Sciences and Technology Division, ‡Academy of Scientific & Innovative Research, CSIR-National Institute for Interdisciplinary Science and Technology, Trivandrum 695 019, India.

The CC bond weakening in MCB has been described in terms of metal-carbon bonding interactions[38] and studies conducted on Grubbs first and second generation MCB systems have shown that the highly electron deficient Ru(IV) in 14-electron configuration interacts directly with both CC σ-bonds.[15] This interaction named as α,β-CCC agostic interaction is found to be a common feature for many MCB systems (M = Ru, Ti, Nb, W, Ta, Zr, Hf, V, Cr, Mo).[15, 37] Experimental electron density studies and NMR studies by Ernst et al. supported the CC agostic interpretation to describe the long CC bonds in titanacyclobutanes.[39-42] Recently Etienne and Weller have reviewed this topic.[43] The agostic bonding and substantial values for the bond order between metal and C_β provided a good explanation for the single bond-like metal-C_β distance (2.2 - 2.4 Å) in MCBs.[15, 37]

The X-ray structure determination of Grubbs metallacycle intermediate is never reported in the literature whereas in the case of Schrock catalyst, several stable tungstenacyclobutanes have been reported. It is also known that depending on the ligand environment and metal centers, the metallacycle can form either trigonal-bipyramidal geometry (TBP) or a square pyramidal (SP) geometry.[4-5, 21, 44-46] Experimental and theoretical studies on these tungstenacyclobutane isomers[4-5, 12, 17-18, 21-22, 25, 27, 47-48] revealed that C_β of the TBP isomer is different from a typical sp3 carbon center as it shows single bond-like metal-C_β distance.

Though the single bond-like RuC_β and WC_β distances in TBP configuration of a metallacycle is described to be well within the range of a typical bonding distance, a clear identification of this type of metal-C interaction as a regular bond is yet to be made. Previously Suresh and Baik have used an arrow originating from an arc that connects the two σ-bonds to illustrate the electron donation to the metal through the unusual α,β-CCC agostic interaction.[15] Proposing a regular bond between metal and C_β in MCB will lead to the immediate identification of a large number of pentacoordinate carbon in organometallic chemistry. The hypercoordination of carbon is a well established phenomenon both experimentally and theoretically.[49-54] Most of the hypercoordinate carbon centres known are either part of an organic system or are coordinated to non-metals.[49, 55-60] Some rare examples of hypercoordination of carbon to metal centres are CLi_5, CLi_6, $HC[Au(PPh_3)]_4^{2+}$ and the iron-molybdenum nitrogenase cofactor.[51, 61-63]

The main aim of this paper is to show that C_β possesses an undeniable amount of pentacoordination in the metallacycle intermediate of Grubbs and Schrock olefin metathesis catalysts. We also attempt to tune the strength of the metal-C_β interaction in the Grubbs systems by varying the ligand environment of the metal center. In certain cases, the RuC_β interaction attains extreme prominence and leads to the formation of a fifth bond path in the quantum theory of atoms-in-molecule (QTAIM) electron density analysis. Further, geometrical, bond order and ^{13}C NMR data will be used to support our arguments to ascertain the fifth coordination of C_β in MCBs. We will start with a systematic study on ruthenacyclobutanes in the TBP and SP configurations. This

will be followed by a study on the X-ray structures reported for tungstenacyclobutanes in the TBP configuration along with a comparison on the SP isomer.

Computational details

All the calculations have been done using Gaussian09 program[64] at the BP86/def2-TZVPP[65-67] level. This level of theory is previously used for the study of metallacyclobutadienes and found to yield structural data in good agreement with experimental results.[68-71] For Ru and W, the def2-TZVPP basis set augmented with effective core potential is used. Vibrational frequency calculation is performed on all optimized structures to verify their minimum energy configuration (zero imaginary frequency). The topological analysis of electron density (QTAIM analysis)[72-74] is done by using the AIMALL program.[75] Wiberg bond order (W_{bo})[76] for all the complexes is calculated using Natural Bond Orbital (NBO) analysis[77] implemented in Gaussian09. For NMR calculation, the Gauge-Independent Atomic Orbital (GIAO)[78-79] method is used.

Results and discussion

Structure of ruthenacyclobutanes

The 14-electron ruthenacyclobutane, the key intermediate of the widely accepted dissociative olefin metathesis mechanism possesses TBP geometry. The halo ligands occupy apical positions of the TBP while the equatorial positions are fulfilled by one N-heterocyclic carbene/phosphine ligand and two RuC_α bonds of the metallacycle. The ligands considered in the present study include fluoro, chloro, bromo and iodo ligands at the apical positions and N-heterocyclic carbene (1,3-bis(methyl)-4,5-dihydroimidazole and 1,3-bis(2,4,6-trimethylphenyl)-4,5-dihydroimidazole), phosphines (PH_3, PH_2Me, $PHMe_2$,PMe_3, and PCy_3) and pyridine ligands at the equatorial positions. The PCy_3 is used in Grubbs first generation catalyst while heterocyclic carbenes are well known in Grubbs second generation catalyst. Sometimes pyridine is used as a leaving group instead of PCy_3 in metathesis catalysts.[80] Further, the effect of methyl substitution on α- carbon atoms of the metallacycle as well as the effect of o-isopropoxyphenyl on one of the α-carbons has been studied. Recently Jaque et al.[26] reported that alkyl substituents at the α-carbons improve the stability of the ruthenacyclobutanes.

The optimized structure of all the 14-electron ruthenacyclobutane complexes **1 − 16** with the general formula $Ru(CR_2CH_2CR_2)X_2L$ where R = H/CH_3/o-isopropoxyphenyl; X = F, Cl, Br, I; L = NHC, PCy_3,Py, NC_5F_5 are shown in Fig. 1 along with the important structural parameters such as $C_\alpha C_\beta$, RuC_α, RuC_β bond distances and $C_\alpha C_\beta C_\alpha$ bond angle. Among these structures **9**, **11**, and **12** are the ruthenacyclobutane intermediates of, Grubbs second, Grubbs-Hoveyda[81] and Grubbs first generation catalysts. The **1 - 16** complexes are characterized by significantly elongated $C_\alpha C_\beta$

bonds (1.581 - 1.612 Å) and RuC$_\alpha$ bonds (1.936 - 2.021 Å) shorter than a typical single bond distance ~2.1 Å. The single bond-like RuC$_\beta$ distance (2.169 - 2.265 Å) is yet another striking structural feature of all these complexes. Further, the C$_\alpha$C$_\beta$C$_\alpha$ bond angle (114.7 - 121.7°) is significantly deviated from the typical C$_{sp3}$ angle 109.5°. All these structural features clearly suggest the existence of unusual metal-carbon bonding interactions in the metallacycle.

Among the fluoro (**1**), chloro (**2**), bromo (**3**) and iodo (**4**) ligated Grubbs second generation metathesis intermediates, the C$_\alpha$C$_\beta$ distance decreases from **1** to **4** in the range 1.589 − 1.581 Å whereas the RuC$_\beta$ and RuC$_\alpha$ distances increase from **1** to **4**; 2.245 − 2.265 Å for the former and 1.948 - 1.975 Å for the latter. These results suggest that with increase in electron rich character of Ru from **1** - **4**, the RuC$_\beta$ interaction decreases.
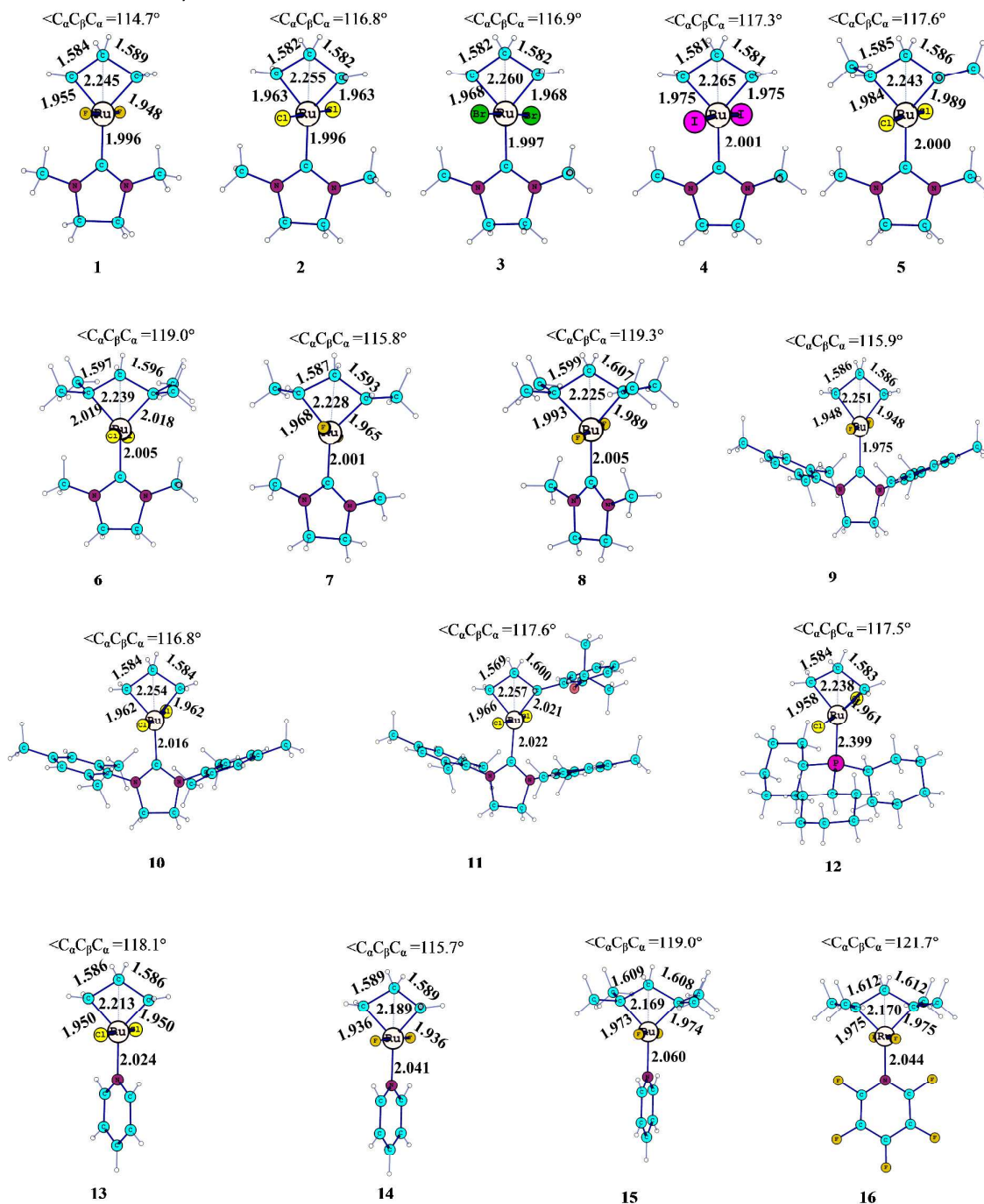

Fig. 1 Optimised geometries of the 14 electron agostic complexes **1 – 16**.

Dalton Transactions Accepted Manuscript

Complex **1** shows a slight amount of puckering at the C_β center with $RuC_\alpha C_\beta C_\alpha$ dihedral angle 14° and in all other cases, the metallacycle is planar. Apart from these geometrical parameters, fluoro ligated system **1** shows a twist angle (θ) 25.8^o between the plane of NHC ring and the plane of the metallacycle defined by Ru and two C_α atoms. The θ, for the chloro, bromo, and iodo ligated systems **2**, **3** and **4** are 18.0, 10.7 and 2.9^o, respectively suggesting that the halo ligands also provide some amount of steric hindrance to the orientation of the NHC ring. In the case of **1**, a CH bond in the methyl substituent shows CH…F interaction with a distance 2.076 Å.

Compared to the unsubstituted **2**, the corresponding methyl substituted **5** at C_α position shows slight elongation of $C_\alpha C_\beta$ and RuC_α bonds and slight compression of RuC_β bond. With dimethyl substitution on each C_α position (**6**), these distance features further enhanced suggesting that methyl substitution on the C_α-position improves RuC_β interaction by lowering the RuC_α and $C_\alpha C_\beta$ interactions. The steric effect of methyl group is obvious in **6** because the unhindered C_β comes closer to the metal center. This aspect is clearly seen in $C_\alpha C_\beta C_\alpha$ angle as a value of 116.8^o in **2** increases to 117.6^o in **5** and 119.0^o in **6**. Very similar structural features can be obtained by comparing the unsubstituted **1** with the corresponding di-methyl substituted **7** or tetra- methyl substituted **8**.

In **9**, **10** and **11**, the NHC ring plane is coplanar to the metallacycle which can be mainly attributed to the steric hindrance offered by the mesityl substituent to the halo ligands as another orientation of the NHC will give rise to electrostatically unfavourable approach of the π-region of mesityl substituent and the lone pair region of the halo ligands. RuC_α bond of **9** is 0.014 Å shorter than **10** whereas RuC_β bond of **9** is only 0.003 Å shorter than **10**. In both cases, $C_\alpha C_\beta$ distances (1.584 and 1.586 Å) are significantly longer than a typical CC single bond. The geometrical features of the Grubbs-Hoveyda intermediate **11** agree close to those of **10** except for the $C_\alpha C_\beta$ bond defined by the o-isopropoxyphenyl bearing α-carbon shows more elongation and the other shows more contraction than the typical values. In the case of Grubbs first generation MCB **12**, the RuC bond distances and the CCC bond angle parameters show close resemblance to the values observed for the second generation MCB **10**. The shorter RuC_β (2.238 Å) bond distance of the Grubbs first generation metallacycle **12** compared to the second generation metallacycle **10** (2.254 Å) is noteworthy.

The pyridine ligated MCB (**13 – 16**) show shorter RuC_α and RuC_β bond distances compared to their analogous phosphine or NHC ligated systems. For instance, in the case of **13**, the RuC_α bond distance 1.950 Å and RuC_β bond distance 2.213 Å are significantly shorter than those of the analogues phosphine complex **12** as well as the NHC complex **2** and **10**. Further, **13 – 16** show more elongated CC bonds than their corresponding phosphine or NHC ligated systems.

Though the dissociative 14-electron pathway is the most widely accepted olefin metathesis mechanism, the associative 16-electron pathway can also lead to CC bond metathesis activity.[13] The ruthenacyclobutane formed in this pathway for

four Grubbs first generation systems (**17, 18, 19** and **20**) and one Grubbs second generation system (**21**) are also considered in this study (Fig. 2). The **17**, **18**, **19** and **20** systems differ only in the type of phosphine ligand used, *viz*. PH_3, PH_2Me, $PHMe_2$ and PMe_3, respectively. This ligand variation is useful to assess the stereoelectronic effect of alkyl substitution on phosphorus. In **21**, the unsubstituted NHC and one PMe_3 phosphine ligand are coordinated to the metal. The **17** - **21** complexes possess octahedral geometry as they show nearly orthogonal orientation of the chloro ligands (ClRuCl angle 79 - 95°). The structural features of the metallacycle region of **17** - **21** are similar to the structural features of the 14-electron metallacycles obtained in the dissociative pathway. They show single bond-like distance parameters for RuC_β (~2.20 Å), unusually long $C_\alpha C_\beta$ single bond distances (1.58 - 1.68 Å) and unusually large $C_\alpha C_\beta C_\alpha$ bond angle (122 - 126°). It is noteworthy that all these features are more dominant in the 16-electron metallacycles than the 14-electron metallacycles.
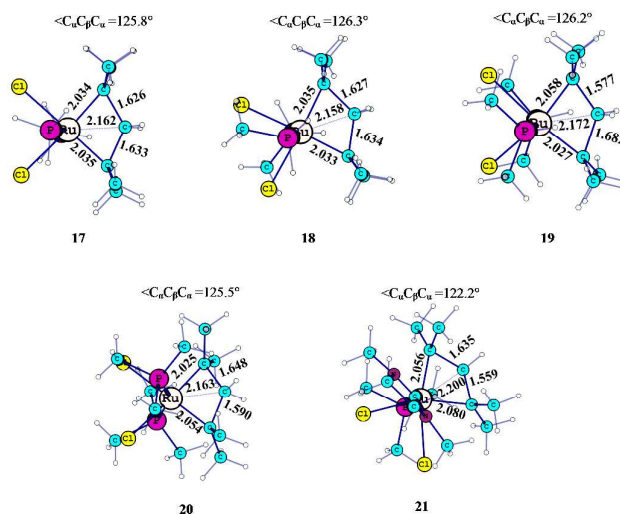
Fig. 2 Optimized geometries of 16-electron agostic complexes.

The unusually long $C_\alpha C_\beta$ bonds in the ruthenacyclobutanes of 14-electron complexes (**1** - **16**) as well as 16-electron complexes (**17** - **21**) can be interpreted on the basis of α,β-CCC agositc interaction.[15] The molecular orbital responsible for the agostic interaction is shown for the 14-electron complex **2** and 16-electron complex **17** (Fig. 3). It appears that the highly electron deficient Ru(IV) in desperate search for electrons finds a way by directly interacting with both the CC σ-bonds.[15] The agostic sharing of the electron density from the CC σ-bonds to the metal leads to significant activation of those bonds in all the complexes (**1** - **21**). At this point, it is imperative to think about the existence of non-agostic isomers of **1** - **21** as they will provide a clear demarcation between the agostic versus non-agostic consequences of structural changes in the metallacycle.

The SP configuration of all the 14-electron metallacycles exists as energy minimum (**1'** - **16'**). These systems show

typical CC single bond distance 1.52 - 1.54 Å and typical RuC_α single bond distance 2.10 - 2.20 Å. Moreover, the RuC_β bond distance of all these structures are significantly longer (2.69 - 2.79 Å) than any of the agostic complexes while their $C_\alpha C_\beta C_\alpha$ bond angle (96 - 102°) is substantially smaller than a C_{sp3} angle. Some representative examples (**2'** and **6'**) showing these structural features are given in Fig. 4 and the rest are given in ESI. These structural data clearly suggest that RuC_β distances are well outside the bonding distances of these atoms, confirming the absence of agostic type interaction in **1'** - **16'**. Hence these systems are described as 'non-agostic complexes' to distinguish them from the agostic isomers **1** - **16**.
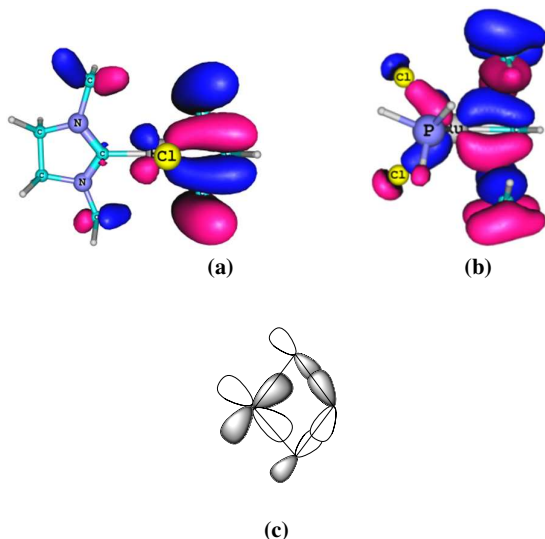

Fig. 3 Molecular orbital showing the α,β-CCC agositc interaction in (a) **2** and in (b) **17**. (c) A schematic diagram showing the orbital overlap between the metal and the CCC region.
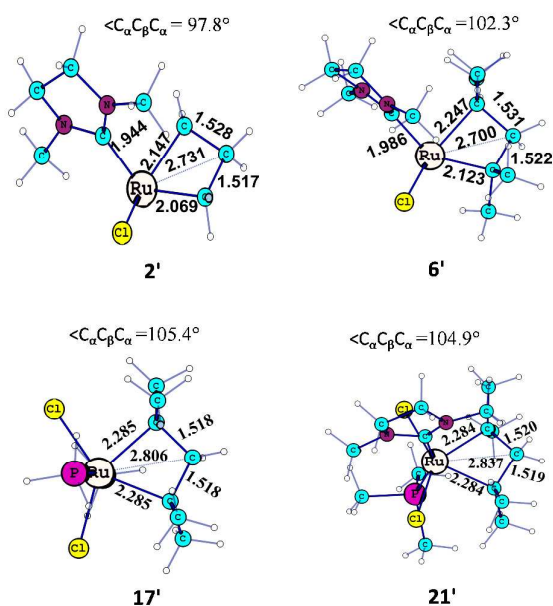

Fig. 4 Optimized geometries of 14- and 16-electron non-agostic complexes.

Among the 14-electron agostic TBP structures and their non-agostic SP isomers, the agostic one is more stable except for the case of **1**. The **1** is 3.21 kcal/mol less stable than the non-agostic isomer **1'** while all other agostic complexes show 1.19 - 15.90 kcal/mol more stabilization than their non-agostic isomers (ESI). Among them the most stable agostic complex is **11**.

It is noteworthy that non-agostic isomers **17'** - **21'** exist for all the 16-electron agostic metallacycles **17** - **21**. These systems show values of CC, RuC_α and RuC_β bond lengths and CCC bond angle very similar to that of 14-electron non-agostic complexes. Two representative examples **17'** and **21'** are depicted in Fig. 4 to illustrate these structural features. One intriguing fact is that the structures of both agostic (**17** - **21**) and non-agostic (**17'** - **21'**) complexes can be described in a distorted octahedral configuration. If we choose the N-heterocyclic carbene/phosphine ligands to define the axial positions of these complexes, the halo ligands and the RuC_α bonds can be used to define the equatorial positions. The distortion from the octahedral geometry is higher in non-agostic complexes than agostic complexes as the former systems show wider ClRuCl bond angle (132 - 165°) than the latter. Mainly these two types of complexes differ in the metal-to-ligand and CC bond distance parameters which suggest the possibility of a rare condition of bond stretch isomerism in organometallics.[82-84] However, such an isomerism can be ignored if we invoke the condition that a fifth bonding between C_β and metal in the TBP configuration exists. Since the bond stretch isomerism is a highly debated subject, and the focus of the paper is on the hypercoordination of carbon, further study on this phenomenon in CC bond metathesis will be presented elsewhere. In the case of 16- electron MCB, all non-agostic models are more stable than the agostic models except **18** by 1.70 - 10.30 kcal/mol (ESI). The **18** is 2.57 kcal/mol more stable than the non-agostic **18'**.

Bond order analysis of ruthenacyclobutanes

Table 1 compares the Wiberg bond order (W_{bo}) for the agostic complexes with that of non-agostic complexes of ruthenium. All the 14-electron agostic complexes show a bond order ~0.20 for Ru and C_β interaction suggesting significant bonding effect. Hence, the single bond-like RuC_β distance observed in these complexes cannot be attributed to the structural restriction imposed by the four-membered ring. The RuC_α bond order above 0.95 is observed for those systems without any substitution in the ring. Once the ring has substitution on the C_α, the RuC_α bond order drops down to 0.931 - 0.869. This indicates steric influence of the substituents on the strength of the bonds. In all the 14 electron agostic cases, the CC bond order (0.932 − 0.858) is less than 1 whereas that of non-agostic complexes (0.99 − 1.03) indicate stronger bonds. The bond order ~0.03 observed for the RuC_β interaction in non-agostic complexes suggests no bonding effect between Ru and C_β.

The RuC_β bond order (0.301 − 0.362) observed for the 16-electron agostic complexes **17** - **21** suggests that the bonding interaction between Ru and C_β is stronger in these systems

than the corresponding 14-electron agostic complexes. The increase in the RuC_β interaction leads to weakening of the CC bonds as they show bond order 0.793 – 0.858. The non-agostic 16-electron complexes **17'** - **21'** show RuC_β bond order ~0.03 suggesting practically no bonding interaction between the two atoms. The correlation plot in Fig. 5 shows that the increased bonding effect between Ru and C_β proportionally decreases the bonding effect between C_α and C_β atoms. This also means that increasing the α,β-CCC agostic interaction increases the bonding effect between Ru and C_β.

Table 1. Wiberg bond order (W_{bo}) values for the agostic **1** - **21** and non-agostic **1'** - **21'** complexes.

| MCB	Agostic			Non- Agostic		
	RuC_α	$C_\alpha C_\beta$	RuC_β	RuC_α	$C_\alpha C_\beta$	RuC_β
1	1.008	0.908	0.190	0.858	1.029	0.025
2	0.995	0.925	0.198	0.852	1.024	0.031
3	0.989	0.928	0.195	0.845	1.025	0.032
4	0.978	0.932	0.191	0.834	1.026	0.032
5	0.931	0.912	0.207	0.787	1.011	0.034
6	0.869	0.895	0.214	0.722	0.994	0.038
7	0.951	0.918	0.201	0.800	1.011	0.024
8	0.893	0.896	0.211	0.760	0.991	0.035
9	1.009	0.932	0.178	0.845	1.026	0.025
10	0.994	0.925	0.197	0.821	1.028	0.029
11	0.919	0.897	0.195	0.761	1.019	0.032
12	0.994	0.924	0.204	0.787	1.030	0.024
13	1.070	0.905	0.251	0.913	1.026	0.036
14	1.085	0.911	0.253	0.886	1.029	0.028
15	0.875	0.866	0.278	0.757	0.999	0.030
16	0.844	0.858	0.294	0.736	1.002	0.029
17	0.783	0.829	0.358	0.674	1.001	0.030
18	0.785	0.823	0.362	0.681	1.001	0.030
19	0.780	0.829	0.347	0.677	1.003	0.031
20	0.777	0.793	0.346	0.674	1.004	0.033
21	0.770	0.800	0.301	0.683	0.996	0.031
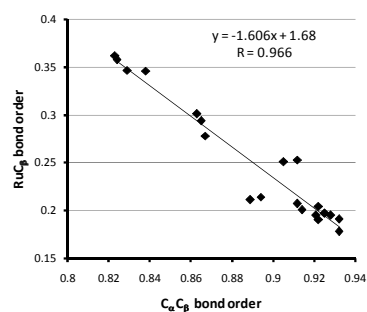
Fig. 5 A linear plot showing the correlation between $C_\alpha C_\beta$ and RuC_β bond orders.

QTAIM analysis

The QTAIM parameters such as electron density (ρ) at the bond critical point (BCP) and ρ at the ring critical point (RCP) for the metallacycle region are given in Table 2. The ρ values in the range 0.135 - 0.158 au and 0.197 – 0.209 au are

respectively observed for the BCP's of RuC_α and $C_\alpha C_\beta$ bonds of **1 – 16** whereas the corresponding values for the non-agostic complex **1' – 16'** are in the range 0.102 – 0.131 and 0.243 - 0.255 au. The ρ values of RCPs clearly indicate that agostic complexes show significant electron concentration (0.070 – 0.083 au) towards the center of the metallacycle than the non-agostic systems (0.052 - 0.061 au).

Table 2. QTAIM parameters for agostic **1** - **21** and non-agostic **1'** - **21'** complexes (all values in au).

MCB	Agostic Complex			Non- Agostic Complex		
	RuC_α BCP	$C_\alpha C_\beta$ BCP	RCP	RuC_α BCP	$C_\alpha C_\beta$ BCP	RCP
1	0.153	0.208	0.073	0.122	0.248	0.059
2	0.149	0.209	0.071	0.119	0.246	0.058
3	0.148	0.209	0.071	0.118	0.246	0.058
4	0.146	0.209	0.070	0.116	0.246	0.057
5	0.143	0.209	0.072	0.113	0.249	0.057
6	0.135	0.206	0.071	0.102	0.246	0.052
7	0.150	0.208	0.074	0.116	0.247	0.055
8	0.142	0.203	0.073	0.111	0.245	0.054
9	0.154	0.207	0.072	0.120	0.246	0.060
10	0.150	0.208	0.072	0.115	0.248	0.058
11	0.140	0.209	0.070	0.109	0.248	0.056
12	0.150	0.207	0.074	0.107	0.252	0.056
13	0.154	0.205	0.077	0.131	0.241	0.061
14	0.158	0.205	0.079	0.127	0.246	0.061
15	0.148	0.199	0.081	0.110	0.243	0.053
16	0.148	0.197	0.083	0.106	0.255	0.052
17	0.129	0.187	0.086	0.086	0.252	0.045
18	0.129	0.187	0.087	0.087	0.252	0.045
19	0.127	0.189	0.083	0.085	0.253	0.045
20	0.127	0.192	0.084	0.084	0.254	0.045
21	0.120	0.202	0.077	0.086	0.250	0.045

The QTAIM molecular graph along with the Laplacian ($\nabla^2 \rho$) contour plots for the metallacycle region in the plane of metallacycle for a representative Grubbs system **2** and its non-agostic isomer **2'** are given in Fig. 6. In the molecular graph, dark green lines correspond to bond paths while pink lines indicate ring paths connecting BCP and RCP. Dashed green curves show area of relative electron concentration and solid blue curves are areas of relative charge depletion. The Laplacian contours of the agostic complexes are markedly different from the non-agostic complexes. It is clear from Fig. 6a that charge concentration from C_β towards the metal center is significant in the agostic complex **2** whereas Fig. 6b shows significant charge depletion from the central region of the metallacycle in **2'**. This argument is supported by the higher ρ value at RCP of **2** (0.071 au) than that of **2'** (0.058 au). In a typical ring system, the ring paths has a sharp meeting point as observed in the case of the non-agostic system **2'** (Fig. 6b) whereas the agostic complex **2** shows a characteristic flat curvature for the ring paths meeting at the RCP (Fig. 6a) and this aspect is clearer in the magnified image of the RCP region of **2** given in Fig. 6c. Although the existence of a bond path is not a necessary condition to describe a bonding interaction between two atoms, a hard-core Bader's fan would have liked

the existence of a bond path between Ru and C_β to unequivocally assign the fifth bond to C_β. To our dismay, none of the 14-electron agostic complexes showed the fifth bond path for C_β whereas all of them showed the characteristic flat curvature of ring paths meeting at the RCP. The $\nabla^2\rho$ plots of **1** - **16** complexes were very similar and markedly different from that of their non-agostic isomers (ESI).
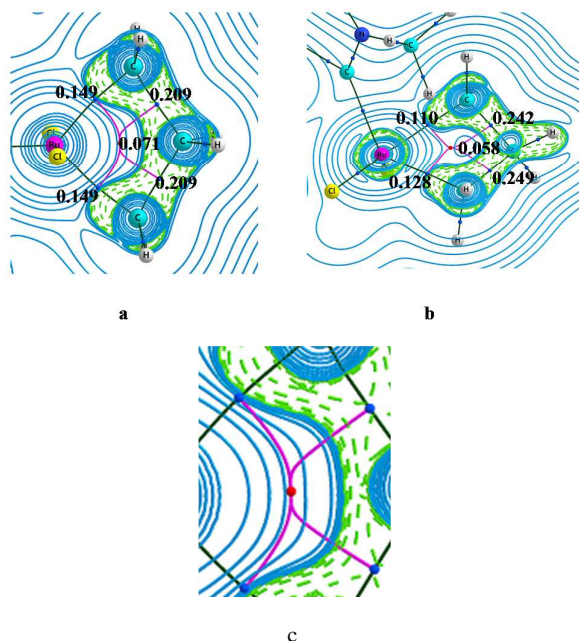

Fig. 6 Contour map of the Laplacian of electron density in the plane of metallacycle for (a) **2** and (b) **2'**. Only metallacyclobutane region is shown for clarity. The ρ values are depicted in au. (c) Magnified image of the RCP region of **2** showing the flat curvature at the meeting point of the ring paths.

Recently Suresh and Frenking reported similar flat curvature for ring paths in the case of metallacyclobutadienes (MCBD) of alkyne metathesis intermediates.[74] They suggested that such a feature is due to the existence of a catastrophe point - a point where both RCP and BCP could merge. They also showed that by restricting the metal-C_β distance to a slightly shorter distance than the optimized one, QTAIM topography of MCBD can exhibit a fourth bond path for C_β along with two RCPs. The fourth bond path named as 1,3-MC bond occupied the same plane of the other three regular bonds (two CC and one CH) and suggested planar tetracoordinate character to C_β in MCBD. We did a similar study in the case of **2** by restricting the RuC_β distance to a value shorter than the optimized value 2.255 Å and found that at RuC_β distance 2.010 Å a BCP emerges for RuC_β bonding interaction along with two RCPs (Fig. 7). The constrained geometry at RuC_β distance 2.010 Å is 11.4 kcal/mol less stable than the equilibrium geometry. The two RCPs and BCP lie very close to each other in the constrained geometry indicating the mergence of these CPs as the RuC_β distance increases to the equilibrium value. This leads to a catastrophe situation which can be seen from the values of the three eigenvalues

(curvatures) of RCP/BCP as one goes from the equilibrium geometry to the constrained geometry (Fig.S1 in ESI). At the equilibrium geometry the three eigenvalues of the (3, +1) RCP are -0.0526, +0.0693 and +0.3000 au. As the RuC_β distance decreases, the positive eigenvalue close to zero becomes smaller and smaller and changes its sign at RuC_β distance 2.010 Å whereas the magnitude of the other two eigenvalues increases. This means that the (3, +1) RCP which represents a minimum ρ point in the plane of metallacycle and maximum ρ point with respect to the path perpendicular to that plane, changes its character drastically to (3, -1) due to a small structural perturbation. At the (3, -1) BCP, the ρ value is minimum with respect to the maximum density path connecting Ru and C_β, but maximum to the rest of the directions. Thus catastrophe nature can be assigned to RCP as this point is at the verge of a critical change in character from (3, +1) to (3, -1). It is also noteworthy that the ρ value 0.113 au for the RuC_β interaction in the constrained geometry is slightly higher than the ρ value 0.110 au observed for one of the RuC_α bond of the non-agostic complex **2'** meaning that by slightly adjusting the RuC_β interaction, one could achieve bonding effect as strong as RuC_α for the RuC_β interaction.
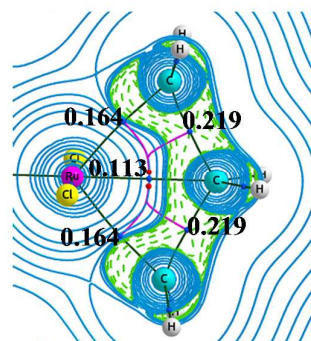

Fig. 7 Contour map of the Laplacian of electron density in the plane of metallacycle for the constrained geometry of **2** showing fifth bond for C_β to Ru. Some portions of the complex are omitted for clarity. The ρ values are depicted in au.

The QTAIM data of the 14-electron agostic complexes in Table 2 and the QTAIM features of the constrained geometry in Fig. 7 clearly suggest that development of significant bonding interaction between Ru and C_β is responsible for the catastrophe character of the RCP. Therefore, it is imperative to assume that the C_β in the agostic complexes possesses a fifth bonding interaction with the metal in addition to the existing two CC and two CH bonds.[38]

To our delight, among the five 16-electron agostic systems studied, the equilibrium geometries of **17** and **18** showed the presence of the fifth bond path between Ru and C_β in QTAIM. The fifth bond path leads to two triangular ring structures defined by Ru, C_α and C_β (Fig. 8). As in the case of the constrained 14-electron agostic complex **2** given in Fig. 7, the two RCPs and the BCP lie very close to each other in **17** and **18**. Further, all these CPs possess nearly same ρ value (0.086 au). The QTAIM data of **17** and **18** clearly suggest that with sufficiently strong interaction between metal and C_β, the

catastrophe RCP in the MCB can be resolved into a BCP and two RCPs. The $\nabla^2\rho$ plots of **17** and **18** are very similar to the 14-electron agostic complexes as well as the 16-electron agostic complexes **19**, **20** and **21** except for the fifth bond path. This suggests that the bonding interaction between Ru and C_β is present in every agostic complex which cannot be ignored due to the absence of a well defined fifth bond path. Instead, the fifth bond of C_β could be judged from the significant build up of electron density at the RCP and its catastrophe character. A well-defined fifth bond path will arise only by very fine tuning of the electron deficiency at the metal center by adjusting the stereoelectronic properties of the ligands.
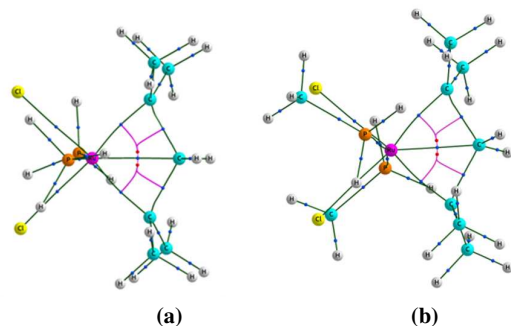

Fig. 8 QTAIM molecular graph of (a) **17** and (b) **18** showing the fifth bond path for the C_β.

In general, QTAIM ρ value of **17** - **21** as well as **17'** - **21'** for RuC_α, RuC_β (either RCP or BCP) and $C_\alpha C_\beta$ bonds (Table 2) agree closely with the corresponding bond order trends (Fig. 9a). Among all the systems discussed so far, **18** has the highest RuC_β bond order (0.362) as well as the highest ρ value at the RuC_β BCP (0.087 au). A decreasing linear trend in W_{bo} with increase in the RuC distance (both α and β carbon atoms) is observed (Fig. 9b). These correlations suggest that QTAIM ρ data is complementary to W_{bo} data. The highest values of the ordered pair of (ρ in au, W_{bo}) data for the RuC_α bond, *viz.* (0.158, 1.085), (0.154, 1.009), (0.153, 1.008) are seen in complexes **14**, **9** and **1**, respectively. For the RuC_β bond, the highest values of (ρ in au, W_{bo}), *viz.* (0.087, 0.362), (0.086, 0.358), (0.084, 0.346) are obtained for complexes **18**, **17**, and **20**, respectively. Thus from the W_{bo} assessment we may conclude that the strength of the fifth RuC_β bond in **18**, **17** and **20** is around 35 % of the strength of the strongest RuC_α bonds in **14**, **10** and **1** whereas the ρ data suggests that RuC_β bond strength is more than half the RuC_α bond strength. The comparison of (ρ in au, W_{bo}) data of RuC_β with that of the weakest RuC_α bonds, *viz.* (0.086, 0.674), (0.084, 0.674), (0.086, 0.683) for **17'**, **20'** and **21'**, respectively suggests that the fifth bond is as strong as RuC_α (from ρ data) or at least half as strong as RuC_α (from W_{bo} data). From all these analyses, it is clear that RuC_β interaction could be called as a fifth bond in all the agostic MCBs. This bonding leads to small RuC_β distance, longer $C_\alpha C_\beta$ bonds and wider $C_\alpha C_\beta C_\alpha$ angles than typical sp^3 hybridized carbon centers. The W_{bo} values and ρ values of the fifth RuC_β bond are in the range 0.18 – 0.36 au and 0.07 - 0.09 au respectively.
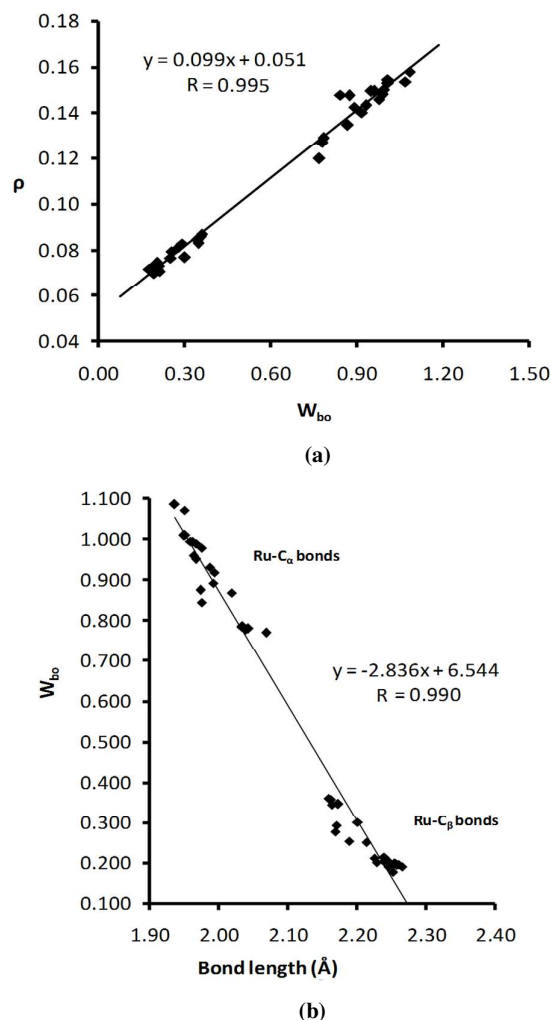

(a)

(b)

Fig. 9 Plots showing correlation of (a) ρ against Wiberg bond order (b) Wiberg bond order against bond length.

Tungstenacyclobutanes

In the case of Grubbs MCB systems, the structural data are available only from computations while metathesis intermediates of Schrock's alkylidene catalysts are well characterized using X-ray crystallography. Hence it would be a nice test to show that the computationally predicted features of the Grubbs systems can be ascertained with the help of metallacycles of similar origin in the Schrock olefin catalysis. We do this comparative study by examining the hypercoordinate state of C_β in known structures of tungstenacyclobutane, available in the Cambridge Crystal Database (CCD).[18, 47, 85-87] The collected structures depicted in Fig. 10 show TBP geometry. The TBP geometries are compared with the X-ray structure of the SP isomer WUWNOR (CCD ID is used to name the crystal structures)[88]. In Table 3, structural parameters of the tungstenacyclobutane region of all these systems are given. All the TBP geometries show single bond-like WC_β distance in the range 2.349 - 2.398 Å, long $C_\alpha C_\beta$ bonds (1.584 - 1.634 Å) and wide $C_\alpha C_\beta C_\alpha$ angle (115 - 118°).

These structural features are very similar to the agostic metallacycles of the Grubbs ruthenium systems and strongly point to the presence of pentacoordinate carbon in the tungstenacycle. Compared to the TBP complexes, the SP complex WUWNOR shows longer WC_β (2.76 Å), longer WC_α (2.17 Å) and shorter CC (1.52 Å) bonds as well as smaller CCC angle (97.3). It is clear that tungstenacycle in the SP configuration is very much like any of the non-agostic ruthenacycles.
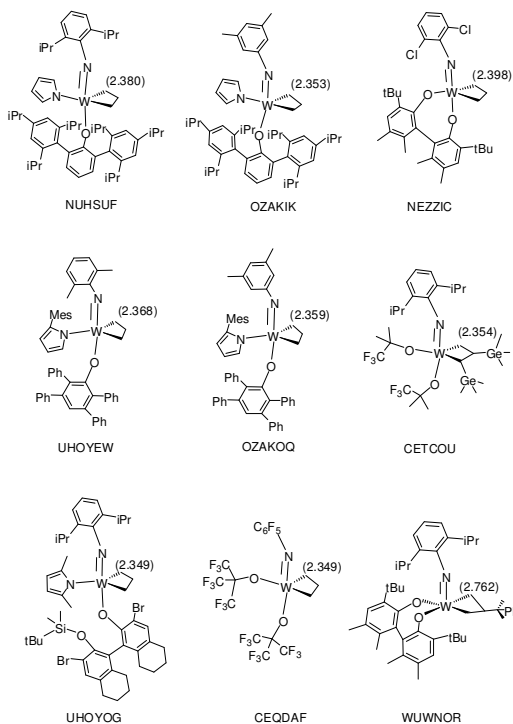

Fig. 10 Schematic structures of tungstacyclobutanes obtained from CCD database. CCD ID is used to name them. The WC_β bond length is given in Å unit in the parenthesis.

Table 3. Structural parameters of the selected crystal structures and models **22** and **23**. Distances are in Å unit and angles in degrees.

MCB	WC_α	WC_α	WC_β	$C_\alpha C_\beta$	$C_\alpha C_\beta$	$<C_\alpha C_\beta C_\alpha$
NUHSUF	2.039	2.037	2.380	1.590	1.634	115.2
OZAKIK	2.070	2.043	2.353	1.600	1.605	118.2
UHOYOG	2.040	2.056	2.349	1.592	1.585	118.0
CETCOU	2.057	2.079	2.354	1.589	1.592	117.3
UHOYEW	2.059	2.057	2.368	1.597	1.603	117.4
OZAKOQ	2.076	2.048	2.359	1.590	1.602	118.3
NEZZIC	2.078	2.016	2.398	1.586	1.584	115.0
CEQDAF	2.042	2.065	2.349	1.604	1.603	118.1
22	2.093	2.082	2.401	1.599	1.604	117.8
23	2.071	2.073	2.379	1.604	1.602	117.8
WUWNOR	2.165	2.169	2.762	1.521	1.528	97.3

We also analyzed the W_{bo} values and QTAIM features of the X-ray structures using the wavefunction obtained from single point energy calculation (Table 4). The W_{bo} values are in the range 0.187 – 0.237 for WC_β, strongly indicating pentacoordination for C_β. Similar to the agostic ruthenacycles,

all the TBP systems showed a catastrophe RCP for the WC_β interaction, but with higher ρ values ($\sim 0.10\ \text{au}$) at the RCP than the ruthenium systems. We also optimized two structures (Fig. 11), one analogous to UHOYEW (**22**) without the isopropyl and methyl substituents on the aromatic rings and the second analogous to CEQDAF (**23**) wherein $-OCF_3$ ligand is used instead of $-OC(CF_3)_3$). The ligand environment of **22** mimics the basic features of NUHSUF, OZAKIK, UHOYOG, UHOYEW and OZAKOQ while **23** mimics the ligand environment of CETCOU, NEZZIC and CEQDAF.

Table 4. Wiberg bond order and QTAIM ρ parameters calculated for tungstenacyclobutanes. Average value is shown for the two WC_α and two $C_\alpha C_\beta$ bonds.

MCB	Wiberg bond order			AIM ρ parameters (in au)		
	WC_α	$C_\alpha C_\beta$	WC_β	WC_α BCP	$C_\alpha C_\beta$ BCP	RCP
NUHSUF	1.001	0.905	0.202	0.195	0.199	0.097
OZAKIK	0.995	0.912	0.200	0.190	0.203	0.099
UHOYOG	1.016	0.912	0.198	0.192	0.209	0.101
CETCOU	0.958	0.927	0.237	0.185	0.206	0.100
UHOYEW	0.990	0.905	0.207	0.187	0.205	0.099
OZAKOQ	0.990	0.905	0.207	0.187	0.207	0.099
NEZZIC	0.985	0.912	0.187	0.195	0.210	0.096
CEQDAF	1.008	0.899	0.227	0.191	0.202	0.102
22	0.985	0.931	0.191	0.180	0.206	0.092
23	1.013	0.923	0.218	0.186	0.205	0.097
WUWNOR	0.841	0.863	0.039	0.165	0.244	0.075
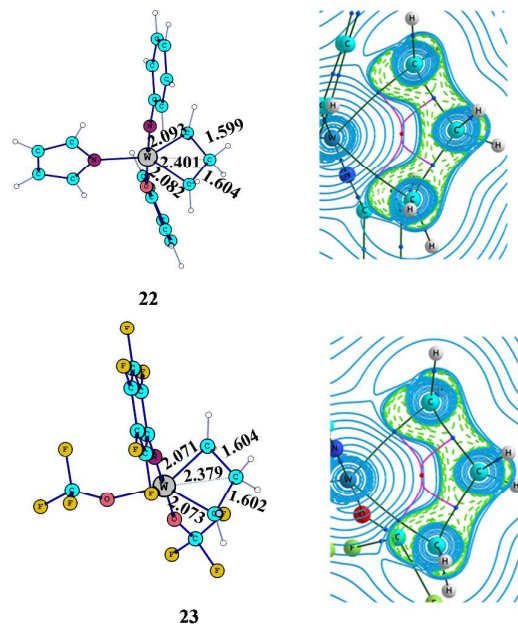
Fig. 11 Optimized geometries and QTAIM Laplacian contour of models **22** and **23**

The optimized structural parameters given in Table 3 for the metallacycle region of **22** and **23** are very similar to that of UHOYEW and CEQDAF, respectively. These data suggest that the single bond-like WC_β distance observed in the X-ray structures cannot be accounted by the crystal packing forces or by invoking the geometrical restrictions (strain) imposed by

the four-membered ring. The QTAIM data and W_{bo} values of **22** and **23** are similar to those reported for the X-ray structures (Table 4). The Laplacian contour plots of **22** and **23** depicted in Fig. 11 illustrate the catastrophe nature of the fifth bonding interaction between W and C_β (the ring paths meet at RCP with a flat curvature). With a slight adjustment of the WC_β distance, the fifth bond path will emerge which is illustrated in the case of **23** in the supporting information (Fig. S10).

NMR analysis

Schrock *et al*. have proposed that significant WC_β interaction in a tungstenacyclobutane can be ascertained from the large difference it shows for ^{13}C NMR signals (δC) of C_α and C_β.[45] Similarly, the strongest evidence to the formation ruthenacyclobutane in Grubbs olefin metathesis is derived from ^{13}C NMR measurements by Romero and Piers[14] who showed that the (δC_α - δC_β) value 92 ppm in **10** is due to significant degree of metal to C_β interaction. Later Rowley et al.[89] theoretically supported this observation and suggested that the large (δC_α - δC_β) value also indicates $C_\alpha C_\beta$ activation. In Table 5, ^{13}C NMR values of the agostic and non-agostic ruthenacyclobutanes are depicted while Table 6 depicts those of the Schrock complexes. The theoretically computed (δC_α - δC_β) value 96 ppm for **10** is only 4 units deviated from the experimental value by Romero and Piers.[14] Similarly (δC_α - δC_β) in the range 94 – 99 ppm is calculated for the unsubstituted Grubbs MCB systems **1**, **2**, **3**, **4**, **9**, **10** and **12**. The Grubbs-Hoveyda system **11** shows (δC_α - δC_β) 99 ppm while that of **5**, **6**, **7** and **8** (methyl substituted at C_α) is 106, 118, 103, 113 ppm, respectively. The pyridine ligated systems **13**, **14**, **15** and **16** show (δC_α - δC_β) values 112, 114, 131 and 141, respectively

Table 5. ^{13}C-NMR data for agostic and non-agostic complexes.

MCB	Agostic			Non- agostic		
	δC_α	δC_β	δC_α - δC_β	δC_α	δC_β	δC_α - δC_β
1	99	5	94	44	36	8
2	104	8	96	41	38	3
3	103	8	95	40	40	0
4	104	8	96	38	41	-3
5	129	23	106	58	57	1
6	154	36	118	81	72	9
7	125	22	103	57	51	6
8	149	36	113	77	67	10
9	101	7	94	39	31	8
10	104	8	96	40	37	3
11	116	17	99	44	44	0
12	106	7	99	33	36	-3
13	114	2	112	78	43	35
14	111	-3	114	57	38	19
15	158	27	131	76	67	9
16	171	30	141	78	63	15
17	172	27	146	88	74	14
18	172	26	146	85	75	10
19	170	26	143	85	76	9
20	171	26	145	83	77	6
21	161	23	138	75	73	2

Table 6. ^{13}C-NMR data for tungstenacyclobutane complexes.

MCB	δC_α	δC_β	δC_α - δC_β
NUHSUF	68	-13	81
OZAKIK	72	-17	89
UHOYOG	75	-16	91
CETCOU	85	3	82
UHOYEW	73	-16	89
OZAKOQ	68	-22	90
NEZZIC	63	-13	76
CEQDAF	77	-16	93
22	83	-3	86
23	90	-3	93
WUWNOR	20	34	-14

indicating that the methyl substitution of the C_α (**15**) and fluorine substitution of the pyridine ligand (**16**) can significantly improve the metal-C_β interaction. The 16-electron MCB systems **17**, **18**, **19**, **20** and **21** show high (δC_α - δC_β) values, *viz*. 146, 146, 145, 143 and 138, respectively. It is noteworthy that **17** and **18** which show the highest (δC_α - δC_β) value possesses the fifth bond path in the QTAIM analysis. Also the computed ^{13}C NMR values of Schrock complexes agreed well with the experimental values.[45] These NMR data clearly suggest that δC_α and δC_β of agostic complexes are markedly different from that for the non-agostic complexes. In the agostic complexes of ruthenium, the (δC_α - δC_β) values are always very large (94 - 146 ppm) compared to the non-agostic complexes (-3 - 35 ppm). Similarly, all the agostic complexes of tungsten show (δC_α - δC_β) in the range 81 - 93 ppm while that of the non-agostic WUWNOR is -14. In general, (δC_α - δC_β) values show a linear trend with respect to the MC_β distance (ESI). These findings are in complete agreement with the earlier conclusions drawn by Schrock *et al*. [45] that a large value of (δC_α - δC_β) is a characteristic feature of metal-C_β interaction in the metallacycles.

Conclusions

Analysis of the structural, bonding, electron density and ^{13}C NMR features of metallacyclobutane (MCB) intermediates of Grubbs and Schrock olefin metathesis catalysts has revealed a unique pentacoordinate state of the C_β in the system. The high oxidation state of metal center in MCB propels the metal center to accept electron density from the CC σ bonds leading to agostic bonding interaction between metal and CC bonds.[37] As a result, single bond-like metal-C_β distance is observed in MCB systems. The fifth bond of C_β to the metal is clearly brought out in terms of significant Wiberg bond order values and appearance of a catastrophe QTAIM RCP in the metallacycle. The ρ at the RCP of Grubbs systems is found to be comparable to the ρ value of a normal RuC bond and for some cases Wiberg bond order values indicated half the strength of a normal RuC bond for the RuC_β bond. In two Grubbs systems, the fifth BCP is clearly observed. Appearance of the catastrophe RCP is proposed as a strong indicator of the fifth bonding interaction between C_β in MCB. To resolve this

Journal Name

ARTICLE

RCP to a BCP, fine tuning of the stereoelectronic properties of the ligand environment is needed. Further, an MCB system showing a catastrophic RCP or fifth BCP is characterized by significantly large (δC_α - δC_β) value than a normal MCB structure. Thus pentacoordination of C_β is strongly supported by ^{13}C NMR data and it also provides an experimental way to monitor the formation of such metallacycles. The pentacoordination of C_β to the metal inherently weakens the CC bonds and facilitates the metathesis reaction.

Acknowledgements

References

1. P. Jean-Louis Hérisson and Y. Chauvin, *Die Makromolekulare Chemie*, 1971, **141**, 161-176.
2. R. H. Grubbs, ed., *Handbook of Olefin Metathesis*, WILEY–VCH Verlag GmbH & Co. KgaA, Weinheim, 2003.
3. T. M. Trnka and R. H. Grubbs, *Acc. Chem. Res*, 2001, **34**, 18-29.
4. J. Feldman, W. M. Davis and R. R. Schrock, *Organometallics*, 1989, **8**, 2266-2268.
5. E. Folga and T. Ziegler, *Organometallics*, 1993, **12**, 325-337.
6. R. R. Schrock, *Tetrahedron*, 1999, **55**, 8141-8153.
7. C. Adlhart, C. Hinderling, H. Baumann and P. Chen, *J. Am. Chem. Soc*, 2000, **122**, 8204-8214.
8. L. Cavallo, *J. Am. Chem. Soc.*, 2002, **124**, 8965-8973.
9. S. F. Vyboishchikov, M. Bühl and W. Thiel, *Chem. Eur. J.*, 2002, **8**, 3962-3975.
10. F. Bernardi, A. Bottoni and G. P. Miscione, *Organometallics*, 2003, **22**, 940-947.
11. P. Chen, *Angew. Chem. Int. Ed.*, 2003, **42**, 2832-2847.
12. R. R. Schrock and A. H. Hoveyda, *Angew. Chem. Int. Ed.*, 2003, **42**, 4592-4633.
13. C. Adlhart and P. Chen, *J. Am. Chem. Soc.*, 2004, **126**, 3496-3510.
14. P. E. Romero and W. E. Piers, *J. Am. Chem. Soc.*, 2005, **127**, 5032-5033.
15. C. H. Suresh and M.-H. Baik, *Dalton Trans.*, 2005, 2982-2984.
16. A. Correa and L. Cavallo, *J. Am. Chem. Soc.*, 2006, **128**, 13352-13353.
17. X. Solans-Monfort, J.-S. Filhol, C. Coperet and O. Eisenstein, *New J. Chem.*, 2006, **30**, 842-850.
18. M. M. Flook, A. J. Jiang, R. R. Schrock, P. Müller and A. H. Hoveyda, *J. Am. Chem. Soc*, 2009, **131**, 7962-7963.
19. A. Poater, F. Ragone, A. Correa, A. Szadkowska, M. Barbasiewicz, K. Grela and L. Cavallo, *Chem. Eur. J.*, 2010, **16**, 14354-14364.
20. X. Solans-Monfort, R. Pleixats and M. Sodupe, *Chem. Eur. J.*, 2010, **16**, 7331-7343.
21. D. V. Peryshkov and R. R. Schrock, *Organometallics*, 2012, **31**, 7278-7286.
22. X. Solans-Monfort, C. Copéret and O. Eisenstein, *Organometallics*, 2012, **31**, 6812-6822.
23. I. W. Ashworth, I. H. Hillier, D. J. Nelson, J. M. Percy and M. A. Vincent, *Acs Catalysis*, 2013, **3**, 1929-1939.
24. Y. Minenkov, G. Occhipinti and V. R. Jensen, *Organometallics*, 2013, **32**, 2099-2111.
25. M. R. Reithofer, G. E. Dobereiner, R. R. Schrock and P. Müller, *Organometallics*, 2013, **32**, 2489-2492.
26. K. Paredes-Gil, X. Solans-Monfort, L. Rodriguez-Santiago, M. Sodupe and P. Jaque, *Organometallics*, 2014, **33**, 6065-6075.
27. X. Solans-Monfort, C. Copéret and O. Eisenstein, *Organometallics*, 2015, **34**, 1668-1680.
28. A. Poater, F. Ragone, A. Correa and L. Cavallo, *Dalton Trans.*, 2011, **40**, 11066-11069.
29. C. A. Urbina-Blanco, A. Poater, T. Lebl, S. Manzini, A. M. Z. Slawin, L. Cavallo and S. P. Nolan, *J. Am. Chem. Soc.*, 2013, **135**, 7073-7079.
30. F. van der EideEdwin and W. E. Piers, *Nat. Chem.*, 2010, **2**, 571-576.
31. S. Vummaleti, L. Cavallo and A. Poater, *Theor. Chem. Acc.*, 2015, **134**, 1-6.
32. S. Manzini, C. A. Urbina Blanco, D. J. Nelson, A. Poater, T. Lebl, S. Meiries, A. M. Z. Slawin, L. Falivene, L. Cavallo and S. P. Nolan, *J. Organomet. Chem.*, 2015, **780**, 43-48.
33. A. Poater, S. V. Chaitanya Vummaleti, E. Pump and L. Cavallo, *Dalton Trans.*, 2014, **43**, 11216-11220.
34. S. E. Vyboishchikov and W. Thiel, *Chem. Eur. J.*, 2005, **11**, 3921-3935.
35. A. Poater, X. Solans-Monfort, E. Clot, C. Coperet and O. Eisenstein, *Dalton Trans.*, 2006, 3077-3087.
36. A. Poater, X. Solans-Monfort, E. Clot, C. Coperet and O. Eisenstein, *J. Am. Chem. Soc.*, 2007, **129**, 8207-8216.
37. C. H. Suresh, *J. Organomet. Chem.*, 2006, **691**, 5366-5374.
38. C. H. Suresh and N. Koga, *Organometallics*, 2003, **23**, 76-80.
39. B. G. Harvey, A. M. Arif and R. D. Ernst, *J. Organomet. Chem.*, 2006, **691**, 5211-5217.
40. B. G. Harvey, C. L. Mayne, A. M. Arif and R. D. Ernst, *J. Am. Chem. Soc.*, 2005, **127**, 16426-16435.
41. S. Scheins, M. Messerschmidt, M. Gembicky, M. Pitak, A. Volkov, P. Coppens, B. G. Harvey, G. C. Turpin, A. M. Arif and R. D. Ernst, *J. Am. Chem. Soc.*, 2009, **131**, 6154-6160.
42. B. G. Harvey, A. M. Arif and R. D. Ernst, *J. Chem. Crystallogr.*, 2011, **41**, 1391-1394.
43. M. Etienne and A. S. Weller, *Chem. Soc. Rev.*, 2014, **43**, 242-259.
44. R. R. Schrock, R. T. DePue, J. Feldman, C. J. Schaverien, J. C. Dewan and A. H. Liu, *J. Am. Chem. Soc.*, 1988, **110**, 1423-1435.
45. J. Feldman, W. M. Davis, J. K. Thomas and R. R. Schrock, *Organometallics*, 1990, **9**, 2535-2548.
46. R. R. Schrock, A. J. Jiang, S. C. Marinescu, J. H. Simpson and P. Müller, *Organometallics*, 2010, **29**, 5241-5251.
47. A. J. Jiang, J. H. Simpson, P. Müller and R. R. Schrock, *J. Am. Chem. Soc.*, 2009, **131**, 7770-7780.
48. A. Poater, X. Solans-Monfort, E. Clot, C. Copéret and O. Eisenstein, *J. Am. Chem. Soc.*, 2007, **129**, 8207-8216.
49. M. Yamashita, Y. Yamamoto, K.-y. Akiba, D. Hashizume, F. Iwasaki, N. Takagi and S. Nagase, *J. Am. Chem. Soc.*, 2005, **127**, 4354-4371.
50. G. K. S. Prakash, G. A. Olah, R. E. Williams, K. Wade, A. Molnár, ed., *Hypercarbon Chemistry*, Wiley-Interscience, New York, 1987.
51. H. Kudo, *Nature*, 1992, **355**, 432-434.
52. E. D. Jemmis, E. G. Jayasree and P. Parameswaran, *Chem. Soc. Rev.*, 2006, **35**, 157-168.

53. Z.-X. Wang and P. v. R. Schleyer, *Science*, 2001, **292**, 2465-2469.

54. K. Ito, Z. Chen, C. Corminboeuf, C. S. Wannere, X. H. Zhang, Q. S. Li and P. v. R. Schleyer, *J. Am. Chem. Soc.*, 2007, **129**, 1510-1511.

55. J. I. Musher, *Angew. Chem. Int. Ed.*, 1969, **8**, 54-68.

56. A. E. Reed and P. v. R. Schleyer, *J. Am. Chem. Soc.*, 1990, **112**, 1434-1445.

57. T. R. Forbus and J. C. Martin, *J. Am. Chem. Soc.*, 1979, **101**, 5057-5059.

58. K.-y. Akiba, M. Yamashita, Y. Yamamoto and S. Nagase, *J. Am. Chem. Soc.*, 1999, **121**, 10644-10645.

59. T. Yamaguchi, Y. Yamamoto, D. Kinoshita, K.-y. Akiba, Y. Zhang, C. A. Reed, D. Hashizume and F. Iwasaki, *J. Am. Chem. Soc.*, 2008, **130**, 6894-6895.

60. W. C. McKee, J. Agarwal, H. F. Schaefer and P. v. R. Schleyer, *Angew. Chem. Int. Ed.*, 2014, **53**, 7875-7878.

61. P. v. R. Schleyer, E. U. Wuerthwein, E. Kaufmann, T. Clark and J. A. Pople, *J. Am. Chem. Soc.*, 1983, **105**, 5930-5932.

62. F. Scherbaum, A. Grohmann, G. Müller and H. Schmidbaur, *Angew. Chem. Int. Ed.*, 1989, **28**, 463-465.

63. K. M. Lancaster, M. Roemelt, P. Ettenhuber, Y. Hu, M. W. Ribbe, F. Neese, U. Bergmann and S. DeBeer, *Science*, 2011, **334**, 974-977.

64. M. J. Frisch, G. W. Trucks, H. B. Schlegel, G. E. Scuseria, M. A. Robb, J. R. Cheeseman, G. Scalmani, V. Barone, B. Mennucci, G. A. Petersson, H. Nakatsuji, M. Caricato, X. Li, H. P. Hratchian, A. F. Izmaylov, J. Bloino, G. Zheng, J. L. Sonnenberg, M. Hada, M. Ehara, K. Toyota, R. Fukuda, J. Hasegawa, M. Ishida, T. Nakajima, Y. Honda, O. Kitao, H. Nakai, T. Vreven, J. A. Montgomery, Jr., J. E. Peralta, F. Ogliaro, M. Bearpark, J. J. Heyd, E. Brothers, K. N. Kudin, V. N. Staroverov, T. Keith, R. Kobayashi, J. Normand, K. Raghavachari, A. Rendell, J. C. Burant, S. S. Iyengar, J. Tomasi, M. Cossi, N. Rega, J. M. Millam, M. Klene, J. E. Knox, J. B. Cross, V. Bakken, C. Adamo, J. Jaramillo, R. Gomperts, R. E. Stratmann, O. Yazyev, A. J. Austin, R. Cammi, C. Pomelli, J. W. Ochterski, R. L. Martin, K. Morokuma, V. G. Zakrzewski, G. A. Voth, P. Salvador, J. J. Dannenberg, S. Dapprich, A. D. Daniels, O. Farkas, J. B. Foresman, J. V. Ortiz, J. Cioslowski, and D. J. Fox, *Gaussian 09, Revision C.01*, Gaussian, Inc., Wallingford CT, 2010..

65. A. D. Becke, *Phys. Rev. A*, 1988, **38**, 3098-3100.

66. J. P. Perdew, *Phys. Rev. B*, 1986, **33**, 8822-8824.

67. A. Schäfer, C. Huber and R. Ahlrichs, *J. Chem. Phys*, 1994, **100**, 5829-5835.

68. C. H. Suresh and G. Frenking, *Organometallics*, 2010, **29**, 4766-4769.

69. C. H. Suresh and G. Frenking, *Organometallics*, 2012, **31**, 7171-7180.

70. C. H. Suresh and G. Frenking, *Organometallics*, 2013, **32**, 1531-1536.

71. A. Poater, E. Pump, S. V. C. Vummaleti and L. Cavallo, *J. Chem. Theory. Comput.*, 2014, **10**, 4442-4448.

72. R. F. W. Bader, *Acc. Chem. Res*, 1985, **18**, 9-15.

73. R. F. W. Bader, in *Encyclopedia of Computational Chemistry*, John Wiley & Sons Ltd., 2002.

74. R. F. W. Bader, ed., *Atoms in molecules: A quantum theory*, Clarendon Press, Oxford, UK, 1990.

75. T. A. K. AIMAll (Version 14.04.17), TK Gristmill Software, Overland Park KS, USA, 2014 (aim.tkgristmill.com).

76. T. K. Brunck and F. Weinhold, *J. Am. Chem. Soc*, 1979, **101**, 1700-1709.

77. F. Weinhold, in *Encyclopedia of Computational Chemistry*, John Wiley & Sons Ltd., 2002.

78. T. Helgaker, M. Jaszuński and K. Ruud, *Chem. Rev.*, 1999, **99**, 293-352.

79. K. Ruud, T. Helgaker, K. L. Bak, P. Jørgensen and H. J. r. A. Jensen, *J. Chem. Phys.*, 1993, **99**, 3847-3859.

80. T.-L. Choi and R. H. Grubbs, *Angew. Chem. Int. Ed.*, 2003, **42**, 1743-1746.

81. S. B. Garber, J. S. Kingsbury, B. L. Gray and A. H. Hoveyda, *J. Am. Chem. Soc.*, 2000, **122**, 8168-8179.

82. P. Gütlich, H. A. Goodwin and D. N. Hendrickson, *Angew. Chem. Int. Ed.*, 1994, **33**, 425-427.

83. Y. Jean, A. Lledos, J. K. Burdett and R. Hoffmann, *J. Am. Chem. Soc.*, 1988, **110**, 4506-4516.

84. G. Parkin, *Acc. Chem. Res.*, 1992, **25**, 455-460.

85. S. Arndt, R. R. Schrock and P. Müller, *Organometallics*, 2007, **26**, 1279-1290.

86. L. N. Bochkarev, Y. E. Begantsova, A. L. Bochkarev, N. E. Stolyarova, I. K. Grigorieva, I. P. Malysheva, G. V. Basova, E. O. Platonova, G. K. Fukin, E. V. Baranov, Y. A. Kurskii and G. A. Abakumov, *J. Organomet. Chem.*, 2006, **691**, 5240-5245.

87. S. C. Marinescu, R. R. Schrock, P. Müller, M. K. Takase and A. H. Hoveyda, *Organometallics*, 2011, **30**, 1780-1782.

88. W. C. P. Tsang, K. C. Hultzsch, J. B. Alexander, P. J. Bonitatebus, R. R. Schrock and A. H. Hoveyda, *J. Am. Chem. Soc.*, 2003, **125**, 6337-6337.

89. C. N. Rowley, E. F. van der Eide, W. E. Piers and T. K. Woo, *Organometallics*, 2008, **27**, 6043-6045.

Table of Contents Artwork and Synopsis

From the analysis of structural, bond order, electron density and ^{13}C NMR data of a large variety of ruthenacyclobutanes and tungstenacyclobutanes, we show that the C_β of the metallacycle is pentacoordinate.

This β-carbon shows five bond paths